Pergamon

Acta mater. 49 (2001) 599–613

Acta MATERIALIA

www.elsevier.com/locate/actamat

DISPERSOID PRECIPITATION AND PROCESS MODELLING IN ZIRCONIUM CONTAINING COMMERCIAL ALUMINIUM ALLOYS

J. D. ROBSON* and P. B. PRANGNELL

Manchester Materials Science Centre, Grosvenor Street, Manchester M1 7HS, UK

(Received 28 August 2000; received in revised form 16 October 2000; accepted 18 October 2000)

Abstract—Small dispersoid particles inhibit recrystallisation and are thus critical in controlling the grain structure of many high strength commercial aluminium alloys. A general, physical model has been developed for the precipitation of Al_3Zr dispersoids in aluminium alloys. The predictions of the model have been compared with results of an experimental investigation of Al_3Zr precipitation in 7050. The model has been shown to faithfully reproduce the distribution of dispersoids observed in this alloy, correctly predicting dispersoid free zones observed in interdendritic regions and at grain boundaries. Furthermore, the predicted precipitation kinetics agree well with experimental observation. The model has been used to study the effects of homogenisation conditions and alloy composition on dispersoid formation and has been shown to be a powerful tool for optimising the dispersoid distribution in 7xxx series aluminium alloys.

Keywords: Computer simulation; Aluminium alloys; Nucleation & growth; Kinetics; Recrystallisation & recovery

1. INTRODUCTION

Small additions of zirconium can often improve the properties of wrought high strength aluminium alloys by forming metastable, coherent Al_3Zr dispersoids which inhibit recrystallisation. The effectiveness of the dispersoids in fulfilling this role depends on their size, spacing and distribution [1]. In commercial practice, the dispersoids are precipitated during homogenisation of the cast billets. The homogenisation conditions are usually chosen to dissolve the maximum number of unwanted eutectic phases and redistribute the solute, rather than optimise dispersoid precipitation. It may therefore be possible to increase the effectiveness of the dispersoids by refining the homogenisation conditions and zirconium concentration.

The binary Al–Zr system has been extensively studied [2–10], particularly in rapidly solidified samples which may have zirconium supersaturations far in excess of those obtained in commercial alloys. It is now well established that, for small zirconium additions, decomposition of the supersaturated solid occurs firstly by the formation of a metastable $L1_2$ Al_3Zr phase [2, 3]. Prolonged heat treatment is usually required before this phase transforms to the equilibrium DO_{23} Al_3Zr phase. Qualitative studies of the precipitation kinetics of the metastable phase in simple, binary alloys show that the peak transformation rate lies between 400 and 500°C [5–7]. The size of the dispersoid particles obtained depends in part on the heat up rate to the homogenisation temperature, with slower heating rates apparently leading to a refinement in particle size [7, 10]. It has also been noted that the Al_3Zr particles are often inhomogeneously distributed within individual grains [10]. This is not surprising, since the dispersoids are precipitating directly from the as-cast state and the initial supersaturation of zirconium varies strongly within the dendritic structure.

A small number of studies have investigated Al_3Zr precipitation in commercial 7xxx alloys. Homogenisation of these alloys leads to the precipitation of the metastable $L1_2$ Al_3Zr phase as fine, spherical particles (typically $\simeq$20 nm in diameter [11, 12]). Dispersoid free zones have been observed in these alloys adjacent to the grain boundaries [11]. This inhomogeneous distribution of dispersoid particles is likely to be of particular significance, since it implies there will be a lower resistance to recrystallisation in regions adjacent to grain boundaries, where the presence of large primary particles is also known to encourage recrystallisation [11].

A key aim of the study was to develop a process

* To whom all correspondence should be addressed. Fax: +44-161-200-3586.

1359-6454/01/$20.00
PII: S1359-6454(00)00351-7

model capable of predicting the dispersoid precipitation during homogenisation. This is of great technological significance, since in principle it should then be possible to determine the optimum composition and homogenisation conditions required to give an improved dispersoid distribution. A physically based model is most satisfying since the number of fitting parameters is usually smallest. Furthermore, physical models often provide an increased understanding of the factors controlling the process. A powerful model can be developed by using well established kinetic equations to calculate the overall transformation kinetics in discreet time steps [13]. At each step, new particles are allowed to nucleate and existing ones grow or shrink depending on their size. The particle size distribution and remaining solute supersaturation are then recalculated and used in making predictions for the change in particle size and number for the next time step. This numerical approach involves tracking the behaviour of a great many particles simultaneously and has therefore only become practical with the advent of high speed computing. The main advantage of this technique is that the traditional regimes of growth and coarsening arise as a natural consequence of changes in composition and driving forces during precipitation. Models based on this approach have been previously applied successfully to a number of systems, including predicting the precipitation of η' in Al–Zn–Mg [14] and calculating the formation of Al_3Li in Al–Li [15].

The precipitation of Al_3Zr in commercial aluminium alloys is complicated by the fact that zirconium segregates during solidification. The Scheil approximation is a simple and widely used method for predicting segregation during casting, which has been shown to give good agreement with experimental observation in aluminum alloys [16]. In this work, a simple Scheil model for the segregation of zirconium was coupled with a model for the precipitation kinetics to allow the local dispersoid size and density to be predicted as a function of position within a grain. This novel combination enables the combined model to successfully predict the inhomogeneities in dispersoid precipitation observed in practice.

The model has been tested by comparing the predictions with experimental results obtained from studying dispersoid precipitation in a commercial 7050 alloy. Electron microprobe analysis has been used to quantify the zirconium distribution in the cast structure. High resolution scanning electron microscopy (FEGSEM) and transmission electron microscopy (TEM) have been used to study the number, size and distribution of dispersoid particles following a range of heat treatments. The advantage using a FEGSEM is that it enables a much larger area from the same sample to be analysed. This has allowed the relationship between the dispersoid precipitation and zirconium segregation to be seen clearly for the first time.

2. EXPERIMENTAL

Specimens, approximately 1 cm cubed in size, were cut from the centre of a slice of stress relieved, direct-chill cast 7050 ingot, supplied by British Aluminium Plate. Stress relief was performed by soaking the ingot for 6 h in a furnace heated to 400°C. The nominal composition of the alloy is shown in Table 1.

Some of the samples of the cast, stress relieved material were then examined in a Cameca SX-50 electron microprobe. Microsegregation of zirconium and other alloying elements was evaluated by performing traverses across 10 grains in each sample, with composition measurements being made at 2 μm intervals.

Isothermal heat treatments were performed on small samples held at temperatures from 350 to 550°C for times ranging from 5 to 100 h. Thermocouples were attached to each sample and used to monitor the metal temperature, which after the initial rapid heating period, was maintained to within ±1° of the target. Following heat treatment, the samples were quenched into cold water.

The heat treated samples were examined in a Philips XL-30 field emission gun FEGSEM. The optimum operating voltage for resolving of the dispersoids was found to be 10 kV using the backscattered imaging mode, where the atomic number contrast due to the zirconium made the Al_3Zr particles easily visible. It was found that with careful specimen preparation and selection of suitable operating conditions, dispersoids as small as 10 nm in radius could be resolved using this instrument.

To investigate the dispersoids formed at short heat treatment times and to enable comparisons to be made between the appearance of dispersoids in the FEGSEM and TEM, thin foils were prepared by electropolishing at 12 V in a 30% nitric acid, 70% methanol solution cooled to −30°C. These were examined in a Philips CM200 TEM operated at 200 kV.

The compositions of the large intermetallic particles, found in both the cast and heat treated condition were measured using energy dispersive X-ray analysis (EDX) in a Philips 525 SEM.

It was found that the size, fraction and spacing of dispersoid particles varied significantly depending upon the position within a grain (see Results). Due to the high magnifications necessary to resolve the small dispersoid particles, only a small fraction of any one grain was imaged at a time. Therefore, great care was taken to examine enough grains, and enough areas within each grain to ensure representative data were collected. For each sample at least 5 grains were examined, and for each grain at least 20 areas were imaged.

3. RESULTS

3.1. Microstructural analysis

Low and higher magnification backscattered electron FEGSEM images of the cast, stress relieved,

Table 1. Nominal composition of the 7050 alloy (wt%) used in the present study

Si	Fe	Cu	Mg	Zn	Ti	Zr
0.03	0.05	2.30	2.30	6.20	0.04	0.13

7050 material are shown in Fig. 1. The grain boundaries can be seen to be delineated by intermetallic constituent particles and eutectic components. EDX analysis has shown that the majority of the intermetallic particles were closest to Al_7Cu_2Fe in composition (Table 2). Within the grains, near the grain boundaries, further plate shaped particles can be seen [Fig. 1(b)]. The morphology and composition of these particles suggests they are η phase. These particles probably precipitate during cooling from the stress relieving treatment.

Typical results of quantitative composition measurements from a linescan across a grain are shown in Fig. 2. In Fig. 2(a) the data have been scaled to allow the different elements to be plotted on the same graph. The peaks in Zn, Cu and Mg correspond to measurements made in, or close to, the intermetallic particles on the grain boundaries. It can be seen that zirconium segregates in the opposite direction to the major alloying elements as expected from a consideration of the peritectic Al–Zr phase diagram [17, 18] and the lowest concentration of zirconium is found at the grain boundaries. The measured actual zirconium concentration across the same grain is shown in Fig. 2(b). The fluctuations in zirconium level across the analysed region reflect the underlying dendritic structure within each grain. The peaks correspond to measurements made close to the centres of the dendrite arms where the zirconium concentration exceeds its nominal value of 0.13 wt%. These regions solidified first during casting and are thus enriched in zirconium. However, a significant fraction of the grain contains zirconium levels below the nominal value. In particular, very low zirconium levels are present near the grain boundaries and interdendritic regions.

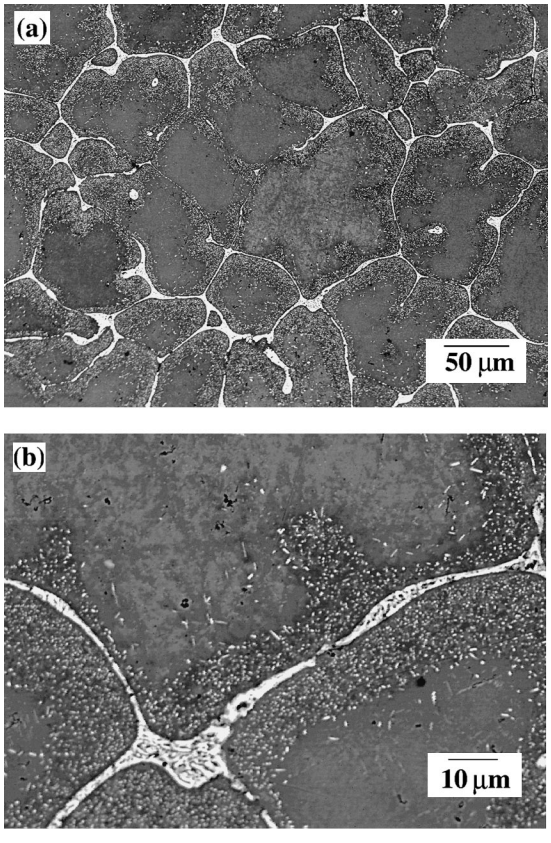

Fig. 1. (a) Low and (b) high magnification backscattered electron images of the as cast structure.

3.2. *Precipitation kinetics*

To obtain an approximate estimate of the dispersoid precipitation kinetics across the range of temperatures investigated, observations were made to determine in which of the heat treated samples Al_3Zr precipitates could be detected. As might be expected, a consequence of the microsegregation of zirconium in the cast material is that the dispersoids were always inhomogeneously distributed within each grain with wide variations in the particle size and spacing. This behaviour is demonstrated for a typical grain in Fig. 3. To enable comparisons to be made after different heat treatments, measurements of the particle sizes were always made from dispersoids in the region close to the centre of the dendrite arms, where the particle size and spacing was most uniform.

Figure 4 shows small dispersoid particles in a dendrite core after heating for 20 h at 450°C as observed using FEGSEM and TEM. The particle radii measured using both imaging methods were similar, as shown in Table 3. This table also summarises for each treatment the measured mean particle radius for samples in which dispersoids were observed. For short times, where no dispersoids were detected in the FEGSEM, TEM observations were made to verify their absence or presence. Of the samples in which no dispersoids were detected in the FEGSEM, only the sample heated for 10 h at 450°C showed evidence of dispersoid precipitation in the TEM.

These results show that the time taken for the dispersoids to reach a given size decreases with increasing temperature, up to at least 550°C (at this high temperature some local melting occurs at the grain boundaries). After only 1 h at 500 and 550°C relatively large dispersoid particles were already present [Fig. 5(a)]. The spherical morphology suggests these are still metastable, rather than equilibrium Al_3Zr.

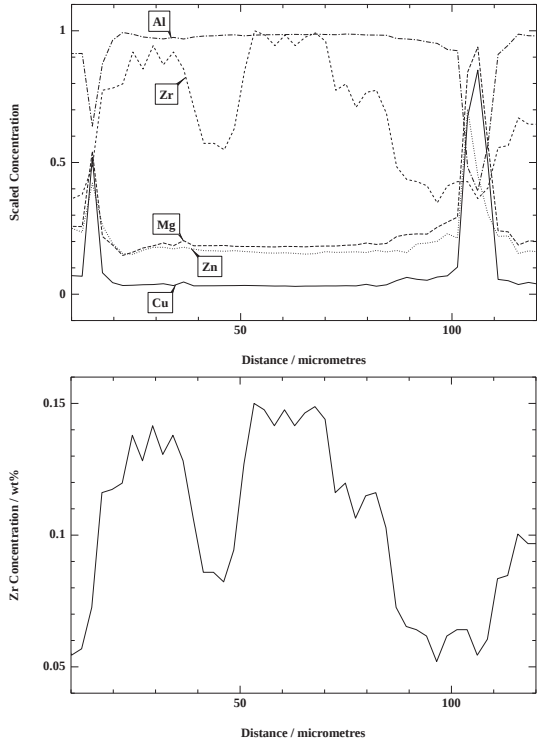

Fig. 2. (a) Scaled variation in the concentrations of Al, Zn, Cu, Mg and Zr across a typical grain. The peaks in Zn, Mg and Cu concentrations correspond to the positions of intermetallic particles at the grain boundaries. (b) Variation in actual zirconium concentration across the same grain.

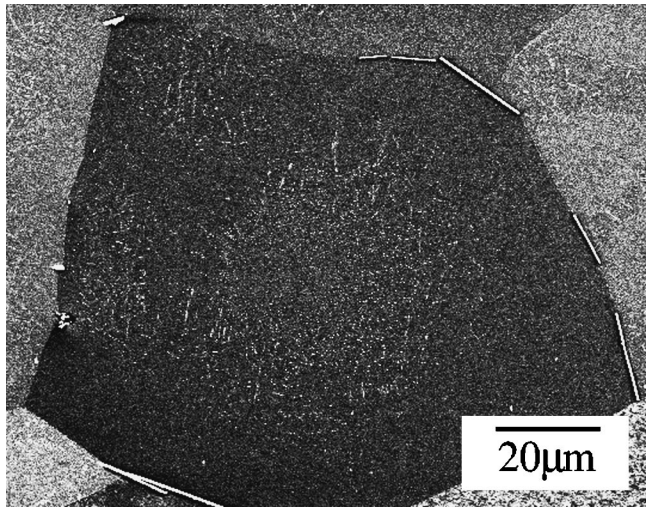

Fig. 3. Image of a grain showing a typical non-uniform distribution of dispersoids after isothermal homogenisation for 20 h at 500°C. At this magnification the dispersoids appear as small, white dots which can just be resolved towards the centre of the grain.

After 20 h at 550°C morphological changes were detected. Many of the dispersoid particles showed orthogonal protrusions [Fig. 5(b)]. These have been noted elsewhere [19] and attributed to preferential growth along ⟨100⟩ and ⟨110⟩ crystallographic directions in the metastable phase. Others showed a cuboid morphology, suggesting transformation to the equilibrium $D0_{23}$ Al_3Zr phase. These particle morphologies were not observed at any of the lower temperatures, even after the longest times. This implies that at 500°C and below, the metastable phase persists for at least 100 h. The observation of the metastable Al_3Zr phase in this alloy (0.13 wt% Zr) at 550°C confirms thermodynamic predictions [18] that the solvus tem-

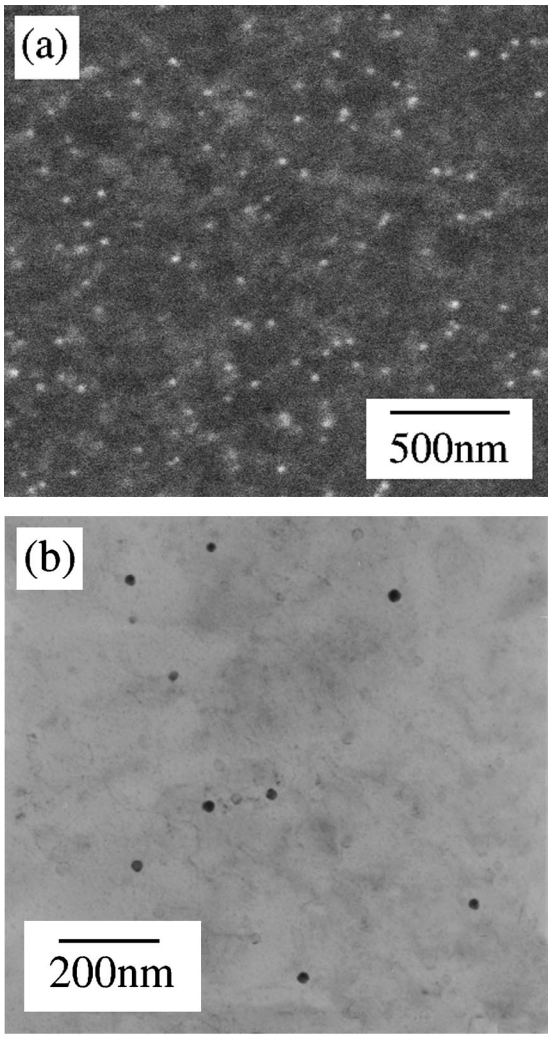

Fig. 4. (a) FEGSEM image of dispersoids after homogenisation at 450°C for 20 h. (b) TEM image of dispersoids in the same sample.

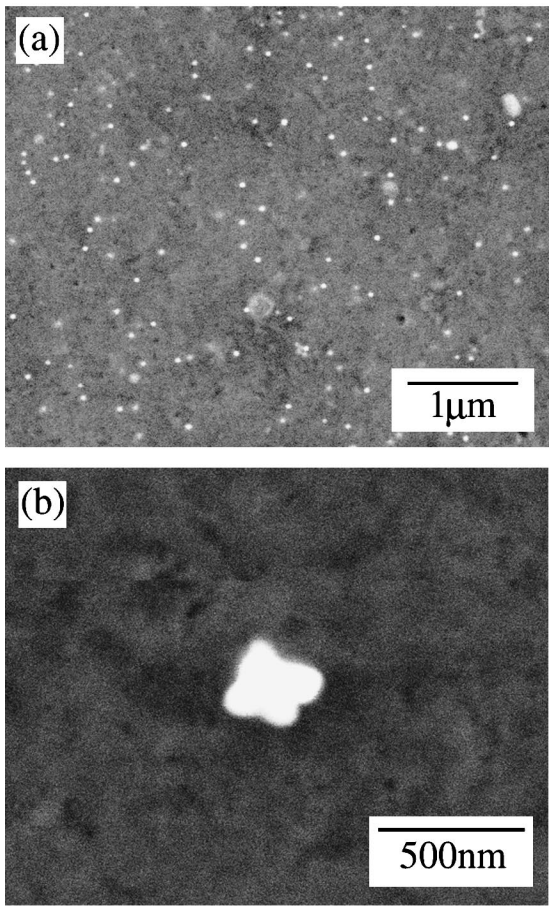

Fig. 5. (a) Al_3Zr dispersoids after homogenisation for 1 h at 550°C. (b) A dispersoid particle after homogenisation for 20 h at 550°C, showing protrusions.

perature of the metastable phase lies close to that for the equilibrium Al_3Zr phase, which is ≃590°C at 0.13 wt.% Zr).

3.3. Influence of zirconium segregation

It has already been noted that the segregation of zirconium during casting leads to wide variations in the dispersoid distribution within each grain. There are also regions, particularly close to grain boundaries, where no dispersoids were observed at all. As expected, the regions where no dispersoids were observed correlate well with with the occurrence of the lowest zirconium levels in the cast structure. The binary phase diagram indicates that dispersoid precipitation will only be thermodynamically possible if the zirconium concentration is greater than about 0.01 wt% at 350°C increasing to over 0.08 wt% at 500°C. With reference to Fig. 2(b), it can therefore be seen that there is insufficient zirconium in solid solution for precipitation of Al_3Zr near to the grain boundaries and interdendritic regions at temperatures greater than ≃400°C. Travelling from the grain boundary towards the centre of a dendrite arm, the zirconium concentration and hence the supersaturation, increases. This results in an increasing driving force for Al_3Zr precipitation. The effect of the local changes in the driving force for precipitation can be seen in Fig. 6(a) where distinctly different precipitation behaviour can be observed depending on the pre-existing solute supersaturation.

Figure 6(a) shows the observed dispersoid distribution in an area adjacent to a grain boundary. Three regions showing different precipitation behaviour may be identified. Close to the grain boundary [region 1, Fig. 6(a)], there are no dispersoids since here the zirconium concentration lies below the solubility limit for the metastable phase. The zirconium in region 3, close to the centre of the dendrites, has a sufficiently high supersaturation after casting to allow the formation of copious numbers of small, homogeneously nucleated, Al_3Zr particles. The most interesting effects occur in region 2. Here, the dispersoid particles are considerably larger (typically twice the radius) than those in region 3 and there are also far

Table 2. Measured mean composition (at.%) of the grain boundary intermetallic particles and the plate shaped precipitates within grains in cast (stress relieved) material. The suggested phase identity is also shown

	Al	Cu	Fe	Mg	Zn	Suggested phase
G.B. precipitate	74.8±6.3	15.0±5.0	7.1±2.5	2.2±0.7	0.76±0.74	Al_7Cu_2Fe
Plates	31.5±7.1	6.3±2.1	0.10±0.10	30.3±3.4	32.7±4.1	η

Table 3. Mean Al_3Zr particle radius (nm) and standard deviation after heat treatment[a]

	1 h	5 h	10 h	20 h	40 h	100 h
550°C	15±3	18±3	—	32±3	—	—
500°C	10±2	12±3	19±5	20±5	20±5	21±3
450°C	X	X	(10±2)	18±2 (20±3)	19±2	25±7
400°C	X	X	X	X	X	10±4
350°C	X	X	X	X	X	X

[a] Diameters shown in brackets were measured using TEM rather than FEGSEM micrographs. (X) indicates no dispersoids were observed. (—) indicates that no measurements were made.

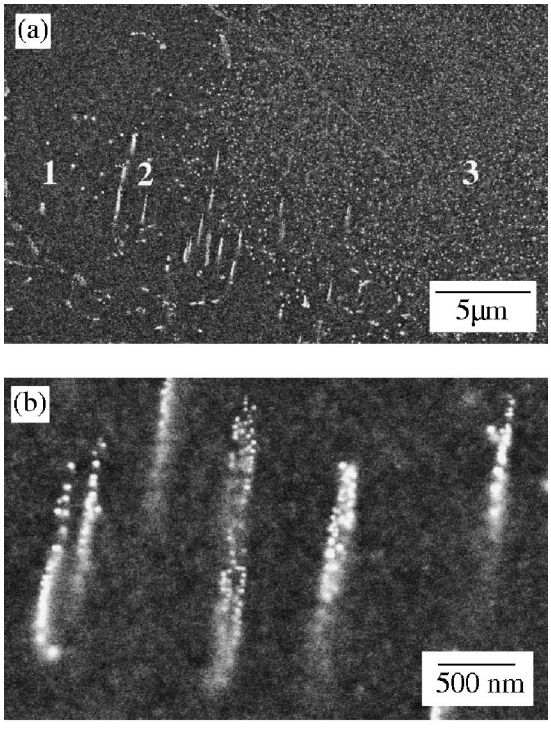

Fig. 6. (a) Pattern of dispersoid precipitation after homogenisation for 20 h at 500°C in a region adjacent to a grain boundary. The boundary itself is to the left of the area viewed. Regions 1, 2 and 3 are referred to in the text. (b) Higher magnification image of clusters of dispersoid particles seen in region 2.

fewer of them. Elongated clusters consisting of groups of 10 or more spherical dispersoid particles can be seen. As region 2 is near to the grain boundary, the supersaturation of zirconium is low and thus the driving force for the precipitation of Al_3Zr is small. A consequence of this is that processes which require a large activation energy will be stifled. However, processes which have smaller energy barriers will still be viable. The relatively low number density of dispersoids observed in region 2 suggests that here the homogeneous nucleation rate, which will be very sensitive to the driving force, is drastically reduced and instead heterogeneous nucleation occurs at preferred sites such as dislocations or pre-existing precipitates. Evidence for nucleation on precipitates is provided by the clusters of dispersoid particles. The location and shape of these clusters correlates well with that of the η precipitates seen in the cast, stress relieved, structure [Fig. 1(b)]. It therefore seems likely that the dispersoids are nucleating heterogeneously on these particles, prior to their dissolution. This observation is not surprising, since it is well known that the reverse behaviour (Al_3Zr acting as heterogeneous nucleation sites for η precipitates) occurs during slow cooling from solution treatment [20, 21]. It is thus apparent that heterogeneous and homogeneous nucleation are competing, with heterogeneous nucleation becoming dominant at low solute supersaturations. This behaviour is, however, dependent upon the availability of suitable nucleation sites.

As well as the regions close to grain boundaries, there were also interdendritic regions within the grains where the zirconium concentration is much lower than the average level. Figure 7 shows a typical

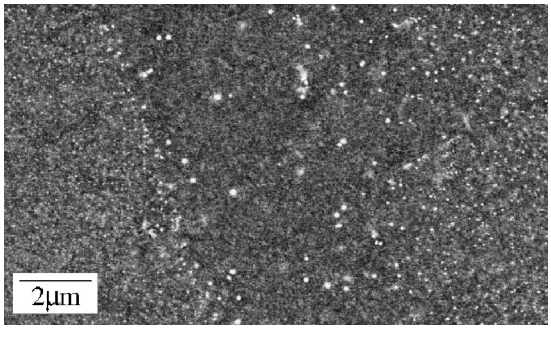

Fig. 7. A dispersoid free region across an interdendritic region within a grain after homogenisation for 40 h at 500°C.

example of the dispersoid distribution in such a region. As noted previously, the zirconium concentration falls below the level required for dispersoid precipitation in the interdendritic region and there is thus a dispersoid free band. In contrast with observations made close to grain boundaries, no clusters of dispersoid particles were observed adjacent to these bands. Instead there was a low number density of large, isolated dispersoids. This lack of dispersoid clusters within the grains arises because the η particles on which they can nucleate were only found near the grain boundaries. The large, isolated dispersoids may therefore be the result of homogeneous nucleation with a low nucleation rate, due to the small zirconium supersaturation. Alternatively they may be heterogeneously nucleated at a feature not yet identified.

The position and width of the dispersoid free regions discussed above depends on the temperature of homogenisation. A decrease in homogenisation temperature will lead to an increased zirconium supersaturation at all points. Therefore, at lower temperatures a narrower dispersoid free region would be expected, providing there is sufficient time for complete precipitation. Nevertheless, even at the lowest temperature where dispersoids were observed to precipitate (400°C), the same general pattern of precipitation was observed and dispersoid free regions, of a similar width, were still present.

4. MODELLING DISPERSOID PRECIPITATION

A model has been developed, based on the methodology of Kampmann and Wagner [13], to predict the influence of zirconium concentration and homogenisation treatment on the precipitation kinetics and distribution of the metastable $L1_2$ Al_3Zr (α') particles. The model for precipitation kinetics has been coupled with data for the segregation of zirconium in the cast structure to enable the dispersoid distribution within a grain to also be predicted.

Development of the model required the use of several simplifying assumptions. These were:

- Metastable Al_3Zr has the stoichiometric composition and is the only precipitate in which zirconium has appreciable solubility. Therefore, its precipitation in 7xxx series aluminium alloys may be adequately modelled by consideration of the metastable phase boundaries in the Al–Zr binary system.
- Nucleation occurs homogeneously within the matrix, with the proviso that the nucleation rate will depend upon the local zirconium concentration. Heterogeneous nucleation on η particles, which was observed in narrow regions close to grain boundaries, has been ignored since such particles are likely to be present only in stress relieved castings.
- The growth of the $L1_2Al_3Zr$ particles is controlled by diffusion of zirconium to the particle/matrix interface.
- The overlap of diffusion fields from adjacent growing particles (soft impingement) may be adequately represented using the mean field approximation.

Subject to these assumptions, nucleation and growth of the Al_3Zr dispersoids can be modelled in a rigorous manner [13]. Particle coarsening, which becomes most important once precipitation is close to completion, arises naturally as a result of the effect of precipitate curvature on the local composition at the particle/matrix interface.

In order to calculate the precipitation kinetics the continuous time evolution is divided up into a discrete number of small time steps of duration Δt. At each step, new particles are allowed to nucleate and existing particles grow (or shrink). The size distribution of the particles is updated accordingly and used to calculate the volume fraction of dispersoids and hence the instantaneous average zirconium concentration in the matrix. The updated mean matrix concentration is then used in calculating the nucleation and growth rates in the next time-step and this procedure is repeated until the desired end-time is reached.

4.1. Nucleation

The classical steady state nucleation equation has been used to describe the nucleation rate. The nucleation rate is then given by [22]:

$$J = N_0 \frac{kT}{h} \exp\left(-\frac{G^* + Q}{kT}\right) \tag{1}$$

where J is the nucleation rate per unit volume. N_0 is the number density of nucleation sites which for homogeneous nucleation is equal to the number of zirconium atoms per unit volume. G^* is the activation energy barrier for formation of a critically sized cluster. Q is the activation energy for diffusion of zirconium in aluminium. k and h are the Boltzmann and Planck constants respectively and T is the thermodynamic temperature. G^* is related to the critical radius and the interfacial energy, σ, according to:

$$G^* = \frac{4}{3}\pi r^{*2}\sigma \tag{2}$$

Following Kampman and Wagner, the critical radius size is calculated using the Gibbs Thomson equation, an approach which is valid for dilute solutions. The critical radius corresponds to a special case of this equation, since when $r = r^*$ the solute concentration at the interface is the same as the mean concentration of the matrix and there is no concentration gradient at the interface. r^* is thus given by:

$$r^* = \frac{2\sigma V_a}{kT \ln \frac{c}{c_\infty^\alpha}} \quad (3)$$

where V_a is the atomic volume, c is the instantaneous concentration of zirconium in the matrix and c_∞^α is the concentration of zirconium in the matrix in equilibrium with Al_3Zr assuming a planar interface. Values of c_∞^α were obtained from the solvus line calculated by Saunders [18] for the metastable Al_3Zr phase in the binary Al–Zr system.

The interfacial energy of the $L1_2$ Al_3Zr particles (σ) is unknown and is the only adjustable parameter in the model. This was determined by finding the best fit between the predicted and experimental results, as will be discussed in the next section.

At each time-step r^* is calculated first (equation 3) and used in conjunction with equations (1) and (2) to calculate the nucleation rate. If it is assumed that the new particles can form anywhere in the assembly (i.e. hard impingement may be ignored) then the number of new particles formed in an interval Δt will simply be ${}^{v}I\Delta t$. The radius of each of the newly formed particles is set to be slightly larger than the critical radius to enable these particles to grow. Following Kampmann and Wagner this radius is arbitrarily taken to be 10% larger than r^*.

4.2. Precipitate growth

Fortunately the $L1_2$ Al_3Zr particles have a simple spherical growth morphology. For spherical particles, the growth rate is given by:

$$\frac{dr}{dt} = \frac{D}{r} \frac{c - c_r^\alpha}{c^{\alpha'} - c_r^\alpha} \quad (4)$$

where D is the diffusion coefficient, r the particle radius, c_r^α the concentration of zirconium in the matrix at the interface (including the effect of the curvature of the interface) and $c^{\alpha'}$ the concentration of zirconium in the particle. c_r^α is calculated from c_∞^α (the mean matrix composition) using the Gibbs–Thompson equation, which for the general case (rather than the special case of $r = r^*$) may be expressed as:

$$c_r^\alpha = c_\infty^\alpha \exp\left(\frac{2\sigma V_a}{kT} \frac{1}{r}\right) \quad (5)$$

The diffusion coefficient of zirconium in aluminium was calculated at a given temperature from:

$$D = D_0 \exp\frac{-Q}{RT} \quad (6)$$

where R is the gas constant. The values for D_0 and Q used were 0.0728 $m^2\ s^{-1}$ and 242 kJ mol^{-1} respectively [23].

4.3. Precipitate coarsening

The radii of particles which nucleate in each time interval are tracked separately. As the fraction of solute in the matrix decreases during precipitation, the critical particle radius increases, reducing the nucleation rate with time. Those particles which have a radius $< r^*$ will have a negative growth rate according to equation (4) and will thus shrink. When the size of a group of particles reaches zero they are removed from the size distribution. In this way, coarsening as well as classical growth is accounted for using these equations.

4.4. Dispersoid distribution within a grain

The experimental observations of dispersoid precipitation demonstrate the strong effect that zirconium segregation has on the eventual distribution of dispersoid particles within each grain. It would be useful to be able to predict this behaviour. Of particular interest is the effect of alloy composition and homogenisation conditions on the width of the dispersoid free zones since these regions are likely to be particularly susceptible to recrystallisation.

Due to zirconium's slow diffusion rate, Al_3Zr dispersoids precipitate before there is time for any long-range diffusional redistribution. This can be demonstrated by a simple $\sqrt{Dt}$ estimate of the mean diffusion distance. For example, even after 24 h at 475°C the zirconium remaining in solid solution will only have diffused $\simeq$0.3 μm. Therefore, to make the predictions, only a knowledge of the variation in zirconium concentration $c(x)$ with distance x prior to homogenisation is required. This is available directly from the microprobe measurements for the 0.13 wt% Zr alloy studied. A simple Scheil model, fitted to microprobe data for the 0.13 wt% Zr alloy, was used to describe the segregation during casting for other zirconium concentrations. The Scheil equation gives the zirconium concentration in the solid (c_s) as a function of the volume fraction solidified (f_s) during casting for one dimensional solidification [24].

$$c_s = k\bar{c}(1 - f_s)^{(k-1)} \quad (7)$$

where $\bar{c}$ is the mean concentration of zirconium and k is the partitioning coefficient. As a first approximation, it was assumed that during solidification f_s increased linearly from 0 to 1 as each dendrite grew outward (a 1-dimensional solidification model). f_s may then be replaced by f_x in equation (7) where f_x is the fractional distance across the dendrite arm from the centre to the edge.

Equation (7) therefore enables composition vs distance profiles to be estimated for any given $\bar{c}$. Using $\bar{c} = 0.13$ wt% for the alloy investigated the predicted profiles were compared with the microprobe measure-

ments. It was found that good agreement could be reached between microprobe measurements and predicted values if the partition coefficient k was taken as being equal to 1.4 (Fig. 8). This value of k was used to predict the composition profile for alloys with other mean zirconium concentrations.

The model for the precipitation kinetics was run repeatedly, using the local zirconium concentrations predicted from the Scheil equation as inputs. In this way, the variation in the mean particle size, number density and volume fraction was predicted as a function of distance from the edge to the centre of the dendrites.

5. DISCUSSION OF PREDICTIONS

5.1. Calibrating the model

The interfacial energy, σ, of the Al_3Zr dispersoids is required in both the expressions for nucleation and growth. Consistent experimentally measured values of this parameter are not available, particularly during the early stages of transformation. The value used for the interfacial energy was therefore found by fitting the predicted values to the experimental results. At 500°C metastable dispersoids were observed after all heat treatment times and thus data from this temperature were used to perform the fitting. The best agreement between predicted and measured particle radii and number density at this temperature was obtained with $\sigma = 0.10$ Jm^{-2} (Fig. 9). This value was then verified across a range of temperatures by comparing the predicted and actual times required for dispersoid observation. To do this, it was assumed that dispersoids were first observed when the maximum particle radius exceeded 10 nm (the radius of the smallest particles observed in practice). Figure 10 shows that the predicted time required for the largest dispersoids to reach this radius is consistent with the observations. The value of 0.1 J m^{-2} for the interfacial energy is within the upper limit of $\simeq$0.2 J m^{-2} expected for a fully coherent nucleus [24].

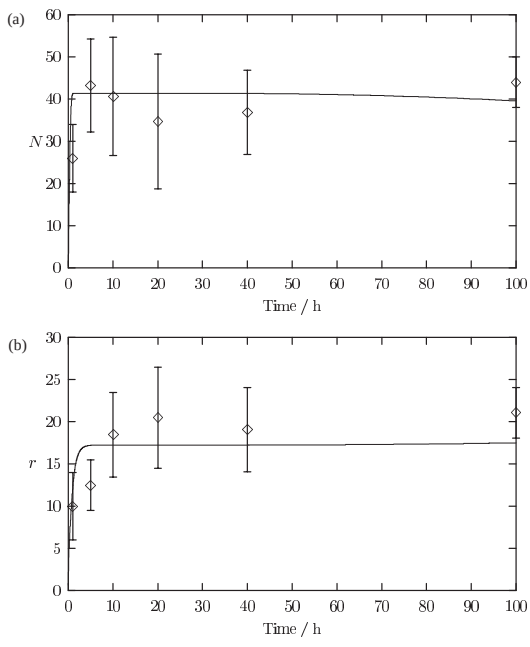

Fig. 9. Predicted evolution of (a) dispersoid number density/μm^{-3} (N) and (b) mean particle radius/nm (r) at 500°C for a zirconium concentration of 0.13 wt%. Experimental data points and associated error bars corresponding to one standard deviation are shown for comparison.

5.2. Predicted TTT behaviour

The predicted time taken for Al_3Zr to reach a given volume fraction (0.05%) is shown on a TTT-diagram in Fig. 11(a) for a zirconium concentration of 0.13 wt%. It can be seen that the most rapid precipitation kinetics are predicted at 495°C which is within the range expected from previous qualitative studies of Al_3Zr precipitation kinetics [6–8]. It is interesting to compare this diagram with that in Fig. 10 which gives the time taken for the dispersoids to reach a certain size. The differences between the two diagrams are best explained with reference to Fig. 11(b). This

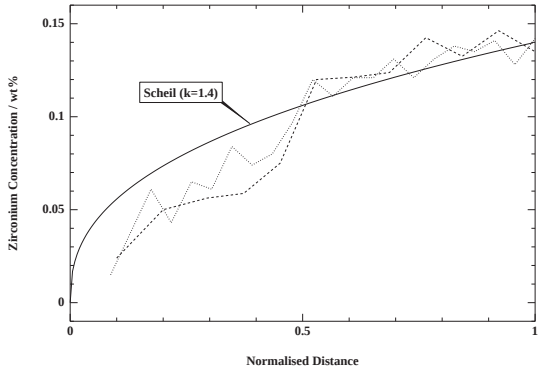

Fig. 8. Zirconium concentration profile from the dendrite edge to the centre predicted by the Scheil model using a partition coefficient (k) value of 1.4. Two measured profiles are shown for comparison.

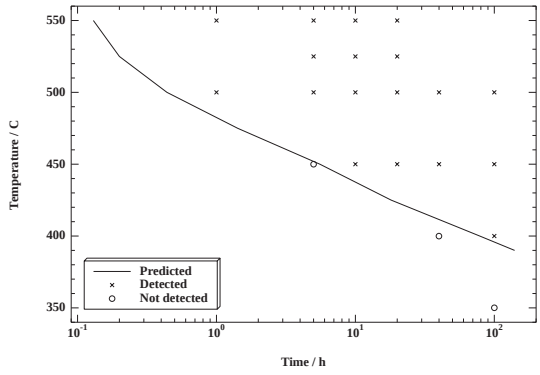

Fig. 10. A plot of the predicted time taken for the maximum dispersoid radius to reach 10 nm for a zirconium concentration of 0.13 wt%, which is approximately the critical size required for detection. Also shown are experimental data points indicating whether any dispersoids were found.

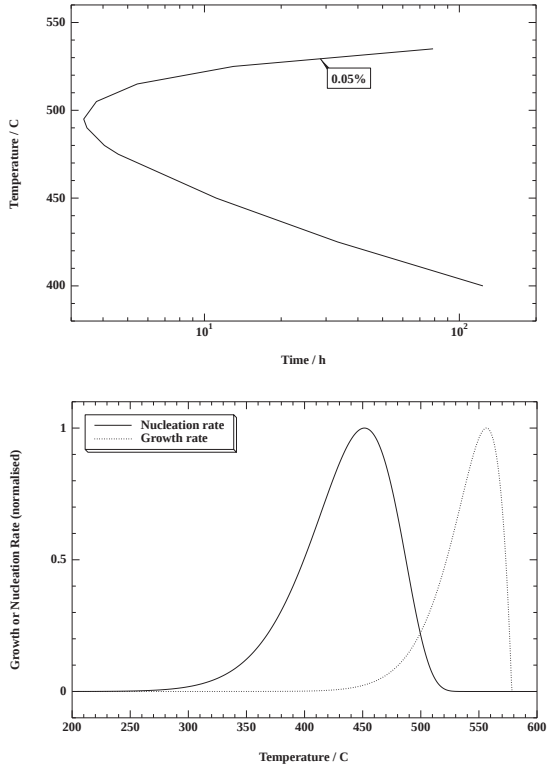

Fig. 11. (a) Predicted TTT diagram for forming a 0.05% volume fraction of Al_3Zr for a zirconium concentration of 0.13 wt%. (b) Variation of the normalized growth and nucleation rates with temperature.

shows how the nucleation and growth rates vary as a function of temperature at the start of transformation. The peak nucleation rate occurs at 450°C and the peak growth rate at 555°C. Thus, at 450°C the highest number of particles will form, but these will grow slowly. At 495°C the optimum balance between the growth and nucleation rates is obtained, giving the fastest kinetics. Above this temperature, fewer particles form, but those which do, grow increasingly rapidly. Therefore the time taken to reach a certain particle size continues to decrease even though the overall transformation kinetics are now slower.

5.3. Optimisation of homogenisation

Precipitation of a uniform fine distribution of dispersoid particles during homogenisation is known to maximise the resistance to recrystallisation [1]. The dispersoid size and spacing will clearly be effected by homogenisation temperature and time. In practice, the range of temperatures and times used are limited since the primary requirement of homogenisation is to dissolve as many of the unwanted intermetallic compounds as possible and redistribute the alloying elements uniformly. To do this, the temperature for

homogenisation must exceed ≃470°C. Although this is predicted to be below the nose of the kinetics "C" curve, it is above the peak in the nucleation rate and is thus not the best temperature for forming the finest dispersoid distribution. In practice, the maximum homogenisation temperature is also limited to below 485°C to avoid liquation of low melting point eutectics. This gives a rather narrow temperature window within which alloys such as 7050 can be homogenised. Figure 12 shows the predicted evolution of dispersoid size and number density with time for a 0.13 wt% Zr alloy homogenised at 475, 480 and 485°C. Despite the small difference in temperature, there is predicted to be a significant effect on the particle density. As expected, the mean radius is predicted to be least and the number density greatest at the lowest temperature, since here the growth rate is smallest and the nucleation rate greatest. When considering the likely effect of a reduction in homogenisation temperature on the recrystallisation resistance, the increased fraction of undissolved large intermetallic particles at low temperature must also be taken into account. Such particles promote recrystallisation by acting as sites for particle stimulated nucleation of new grains [11]. This effect will therefore compete with the increased Zener pinning expected due to a refined dispersoid distribution.

It has previously been reported that slow heating rates up to the homogenisation temperature lead to a refinement in dispersoid size [7, 10]. In commercial practice, slow heating will arise naturally due to the thermal mass of the ingot, the centre heating up more slowly than the surface. The model was used to investigate the effect of heating rate on the dispersoid size and number density. Figure 13(a) shows the variation of the predicted mean radius with heating time for a high temperature homogenisation treatment of 480°C for 24 h at temperature. It can be seen that a modest refinement in size, from a mean radius of 17 nm to a mean radius of 14 nm is predicted for ramp heating over 40 h rather than the isothermal treatment. However, the particle number density increases more sharply and almost doubles. In Fig. 13 it can be seen that if even longer heat up times are used, some further refinement is predicted, but the sensitivity to heating rate drops.

Changing the average zirconium concentration of the alloy would be expected to lead to changes in the dispersoid radius and number density. The specification for alloy 7050 allows for zirconium in the range 0.08–0.15 wt%. The predicted effects of varying the zirconium level in this range on the mean particle size and number density are shown in Fig. 13(b). In commercial practice, it is unlikely that a zirconium level as high 0.15 wt% can be retained in solid solution after casting due to precipitation of primary Al_3Zr. This calculation also only reflects the "average" behaviour since segregation leads to large local

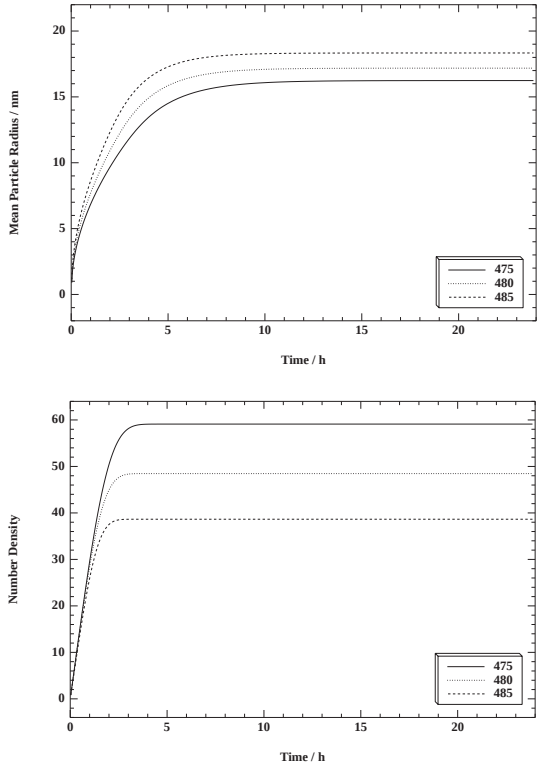

Fig. 12. (a) Predicted evolution of mean radius and (b) dispersoid number density/μm^3 with time for three different homogenisation temperatures.

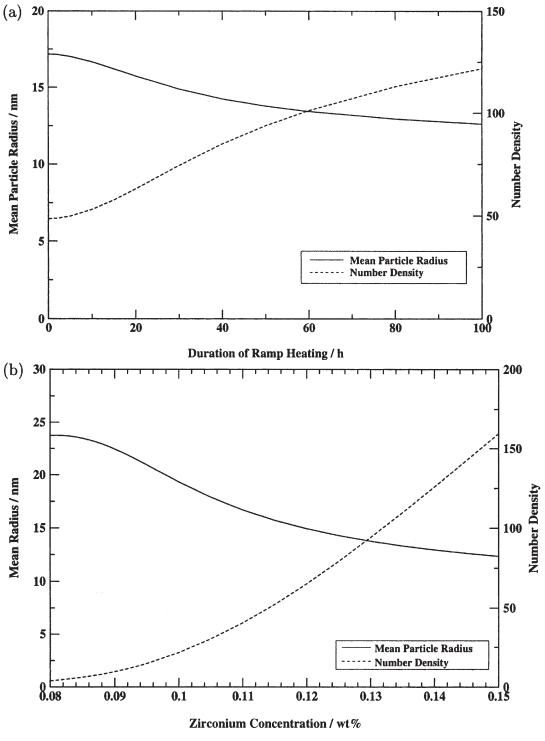

Fig. 13. (a) Predicted effect of heat up time to homogenisation (24 h at 480°C) on the number density/μm^3 and mean radius of the dispersoids. (b) Predicted number density/μm^3 and mean particle radius as a function of zirconium concentration after homogenisation for 24 h at 480°C (allowing a 20 h heat up time).

fluctuation in zirconium concentration. As expected, it is predicted that increasing the zirconium content leads to a greater number of dispersoid particles, since the driving force for nucleation increases. From Fig. 13(b) it can be seen that there is a wide variation in the number density of particles in going from the lowest to the highest zirconium concentration. This reflects the large range of zirconium concentration permissible in 7050 and the high sensitivity of nucleation rate to supersaturation. The predicted variation in the mean dispersoid radius shows the opposite trend. This behaviour results from the competition for the available solute between growth and nucleation. At higher zirconium levels, the nucleation rate is large and many particles form, each of which is only able to grow to a small size before exhausting the supersaturated zirconium. As the zirconium level falls, the nucleation rate falls more sharply than the growth rate. Since far fewer particles are forming, each particle can grow to a larger size before exhausting the supersaturated zirconium, despite there being a lower zirconium concentration. This agrees with the experimental observations which show an increased particle size as the local zirconium concentration falls towards the edge of the dendrite arms (e.g. Fig. 7). The average grain boundary pinning pressure of the dispersoids in a 0.08 wt% alloy is therefore expected to be several orders of magnitude smaller than that in a 0.15 wt% Zr alloy.

5.4. Dispersoid distribution within a grain

Experimental observations have shown that the dispersoids are heterogeneously distributed within each grain. This has been attributed to variations in the local zirconium concentration resulting from segregation during casting. The model was therefore used to make predictions of the volume fraction, mean particle radius and number density as a function of position, using the concentration profile fitted with the Scheil equation. Figure 14 shows the predicted variation in dispersoid size and number from the edge to the centre of a dendrite after isothermal homogenisation for 20 h at 480°C. The model correctly predicts a dispersoid free region at the dendrite edge. This is followed by a transition region with a small number of particles with a relatively large mean radius. At the highest zirconium concentrations the particle number density increases and the size decreases. All of these phenomena are consistent with the experimental observations [Fig. 6(a)]. However, heterogeneous nucleation of dispersoids is not accounted for in the model. Thus, the predicted number density in regions where heterogeneous nucleation occurs is likely to be an underestimate.

The dispersoid free regions are likely to recrystallize most easily, as has been noted by previous workers [11]. Therefore, reducing the width of these regions is expected to lead to a beneficial decrease in the fraction of recrystallisation. Homogenising at a lower temperature will increase the zirconium supersaturation at all points across the grain and thus dispersoids should form at a lower zirconium level, providing the kinetics of precipitation are sufficiently rapid at the lower temperature. Increasing the average zirconium concentration will similarly increase the supersaturation, although the magnitude of the increase will also depend on how the zirconium seg-

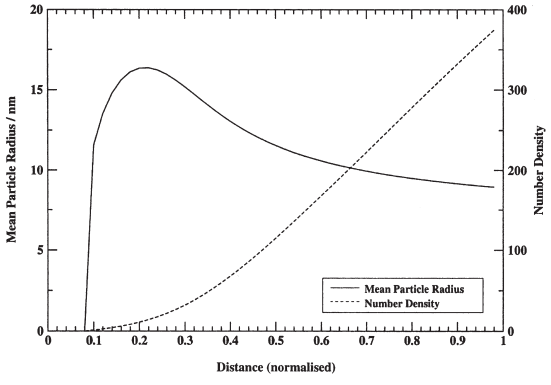

Fig. 14. Predicted number density/μm^3 and mean particle radius as a function of the normalized distance between dendrite edge and centre after homogenisation for 24 h at 480°C (allowing a 20 h heat up time).

regates. Figure 15 shows the predicted effects of homogenisation temperature, average zirconium concentration and heating rate (within commercially possible ranges) on the variation in volume fraction of the dispersoid phase for a standard homogenisation time of 24 h. It can be seen from Fig. 15 that changing the homogenisation temperature has a fairly small effect on the width of the dispersoid free region. This is because there are two competing effects at work. At lower homogenisation temperatures, the supersaturation of zirconium is increased and thus precipitation of dispersoids is thermodynamically possible at a lower zirconium level (i.e. closer to the dendrite edge). However, the kinetics of precipitation are slower at the lower temperature. The model predicts that the kinetic effect outweighs the thermodynamic effect; i.e. the dispersoid free region is slightly wider at lower temperature because there is insufficient time for complete precipitation, despite the increased supersaturation. The Scheil model was then used to predict the concentration profiles for mean zirconium levels of 0.11 wt% and 0.09 wt%. The predicted effect of the three zirconium levels on the variation in dispersoid volume fraction is shown in Fig. 15(b). It can be seen that relatively small reductions in the average zirconium level are predicted to lead to a substantial increase in the width of the dispersoid free region. For example, a decrease in zirconium concentration from 0.13 to 0.09 wt% is predicted to double this width.

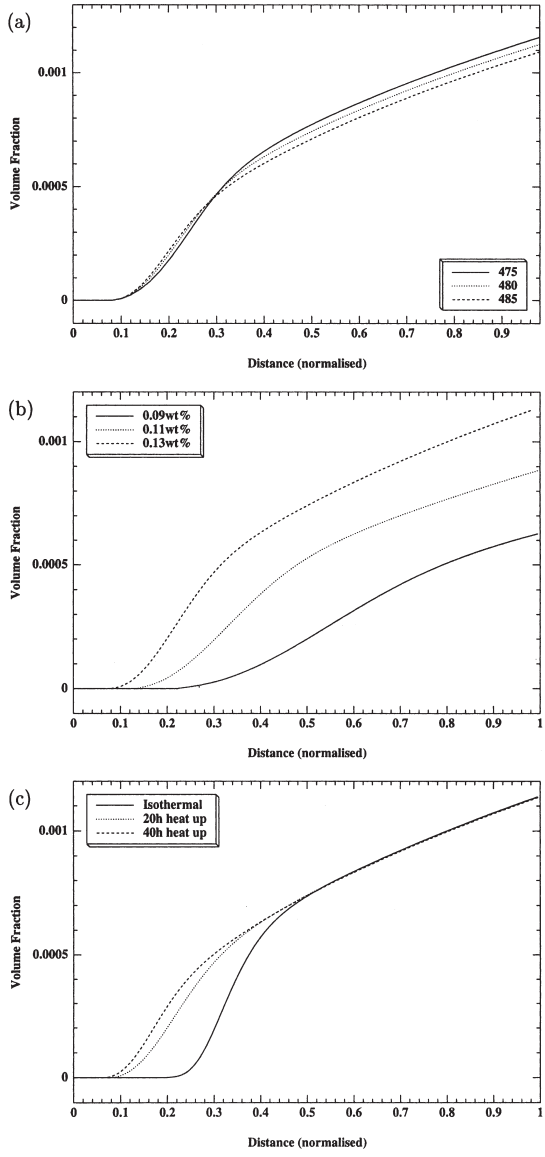

Fig. 15. Prediction of the volume fraction of dispersoids as a function of the normalized distance between dendrite edge and centre after 24 h homogenisation. (a) Three homogenisation temperatures (0.13 wt% Zr, 20 h heat up time). (b) Three mean zirconium levels (480°C homogenisation, 20 h heat up time). (c) Comparing isothermal and ramp heating (0.13 wt% Zr, 480°C homogenisation).

Ramp heating, at a sufficiently slow rate, would also be expected to reduce the width of the dispersoid free region due to the increased zirconium supersaturation and hence enhanced particle nucleation during heating. The predicted effect of three different ramp rates is shown in Fig. 15(c). It can be seen that compared with isothermal treatment, ramp heating leads to a significant decrease in the width of the dispersoid free region. There is, however, little advantage to be gained from use of a heat up time longer than 20 h.

The model was further used to predict the pattern of dispersoid precipitation across an interdendritic region within a grain and compare this with experimental observation. In Fig. 16(a), a plot is given of the measured zirconium concentration across such a region prior to homogenisation. Figure 16(b) is a plot of the predicted dispersoid number density and mean radius across the same region following homogenisation at 500°C for 40 h. These predictions were compared with the observed pattern of dispersoid precipitation in the same region after an identical heat treatment (Fig. 6). The model has correctly predicted that as the zirconium concentration falls, the number density of particles decreases and the mean radius increases to reach a peak, resulting in a narrow band of large particles. On further reduction of the zirconium, the predicted number density falls to almost zero, corresponding to the dispersoid free region. It is interesting to note that the observed increase in mean particle radius in the regions of intermediate zirconium concentration is predicted to occur even if nucleation in these regions still occurs homogeneously. This behaviour is a result of the relative changes in the growth and nucleation rate with zirconium concentration, as discussed previously.

6. CONCLUSIONS

The precipitation of metastable Al_3Zr dispersoids has been studied in a commercial aluminium alloy in which there is strong microsegregation of zirconium. These results have been compared with a model

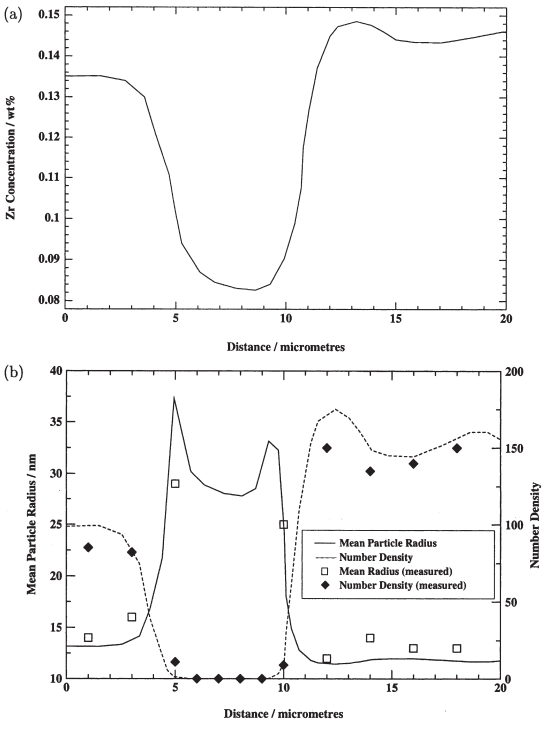

Fig. 16. (a) Measured zirconium concentration across an interdendritic region within a grain after casting. (b) Predicted and measured particle number density and mean dispersoid radius across the same region after homogenisation for 40 h at 500°C.

developed in order to optimise the homogenisation treatment of commercial castings.

1. Strong zirconium segregation towards the dendrite centres occurs during the casting of a commercial 7050 aluminium alloy.
2. The pattern of dispersoid precipitation observed within a grain after homogenisation treatment depends critically on distribution of zirconium. In low zirconium regions, the solubility limit is not exceeded and no dispersoids precipitate. At intermediate zirconium levels, a low density of large particles form, which nucleate heterogeneously on dislocations or η particles where present. In regions of higher zirconium, a fine distribution of homogeneously nucleated dispersoids is observed.
3. A physical model has been developed to describe the kinetics of precipitation and distribution of metastable Al_3Zr dispersoids. The model has general applicability and has been shown to reproduce the experimental observations well for a commercial 7050 alloy. The model provides a powerful tool in predicting the effects of changes in alloy composition and homogenisation practice on the dispersoid distribution.
4. Use of a lower homogenisation temperature and ramp heating are predicted to lead to a modest reduction in particle size and a significant increase in number density. This is expected to increase the effectiveness of the dispersoids in pinning grain boundaries. Large changes in dispersoid size and number density (and therefore pinning effect) are predicted for variations in zirconium concentration within the range allowed for in commercial alloy specifications.
5. Interdendritic and grain boundary free regions are known to recrystallise the most readily. It is predicted that the width of the dispersoid free regions is almost unchanged by altering the homogenisation temperature. Use of slow heat up rates to the homogenisation temperature and an increase in zirconium concentration both reduce the predicted dispersoid free width. The zirconium concentration is predicted to have the most potent effect, with a small increase in zirconium concentration leading to a large reduction in the dispersoid free width.
6. The predictions imply that to obtain a dispersoid distribution which leads to a minimum fraction of recrystallisation requires a zirconium concentration near the upper limit (e.g. 0.13 wt% Zr) and slow heating to the homogenisation temperature, with a heat up time of 20 h being sufficiently long. Since the width of the dispersoid free region is predicted to be insensitive to small changes in homogenisation temperature, this should be chosen to fully dissolve the soluble intermetallic particles.

Acknowledgements—The authors are grateful to The Luxfer Group for funding this work. They also thank J. Newman and S. Khosla of Luxfer for their invaluable help and advice.

REFERENCES

1. Humphreys, F. J. and Hatherly, M., *Recrystallisation and Related Annealing Phenomena*, Pergamon. Oxford, 1995.
2. Nes, E., *Acta metall.*, 1972, **20**, 499.
3. Ryum, N., *Acta metall.*, 1969, **17**, 269.
4. Chen, Y. C., Fine, M. E. and Weertman, J. R., *Acta metall. mater.*, 1990, **38**, 771.
5. Izumi, O. and Oelschlagel, D., *Scripta metall.*, 1969, **3**, 619.
6. Rystad, S. and Ryum, N., *Aluminium*, 1977, **53**, 193.
7. Sato, T., Kamio, A. and Lorimer, G. W., in *Proc. 5th Conf. Alumininum Alloys (ICAA-5)*, Vol. 2, 1996, p. 895.
8. Sato, T. and Kamio, A., in *Proc. Conf. on Science and Engineering of Light Metals*, Vol. 1, 1997, p. 977.
9. Westengen, H., Auran, L. and Reiso, O., *Aluminium*, 1981, **57**, 797.
10. Deischer, H. P., Rumplmair, G., Lacom, W. and Katner, F., *Electron Microscopy*, 1984, **1**, 753.
11. Engler, O., Sachot, E., Ehström, J. C., Reeves, A. and Shahani, R., *Mater. Sci. Tech.*, 1996, **12**, 717.
12. Yoshida, H. and Baba, Y., *Trans. Jap. Inst. Metals*, 1982, **23**, 620.
13. Kampmann, R. and Wagner, R., in *Materials Science and Technology: A Comprehensive Treatment*, Vol. 5 VCH, Weinheim, 1991, p. 213.
14. Deschamps, A., Bréchet, Y. and Guyot, P., in *Proc. 7th Int. Seminar IFHT*, 1999, p. 365.
15. Sigli, C., in *Proc. 7th Int. Conf. Aluminium Alloys (ICAA-7)*, Vol. 1, 2000, p. 513.
16. Saunders, N., in *Minerals, Metals and Materials Soc. AIME (USA)*, 1997, p. 911.

17. Murray, J., Peruzzi, A. and Abriata, J. P., *J. Phase Equilibria*, 1992, **13**, 227.
18. Saunders, N., *Z. Metallkde.*, 1989, **80**, 894.
19. Hori, S., Saji, S. and Kobayashi, T., *Tech. Report Osaka Uni.*, 1978, **28**, 359.
20. Conserva, M. and Fiorini, P., *Metall. Trans.*, 1973, **4**, 857.
21. Kolkman, H., t'Hart, W. G. J. and Schra, L., in *Strength of Metals and Alloys (ICSMA-5)*, Vol. 2, 1998, p. 597.
22. Christian, J. W., *Theory of Phase Transformations in Metals and Alloys*, Pergamon, Oxford, 1975.
23. Zedalis, M. S. and Fine, M. E., *Metall. Trans. A*, 1986, **17**, 2187.
24. Porter, D. A. and Easterling, K. E., *Phase Transformations in Metals and Alloys*. Chapman and Hall, London, 1992.